Asian Journal of Chemistry; Vol. 35, No. 11 (2023), 2659-2667

ASIAN JOURNAL OF CHEMISTRY

https://doi.org/10.14233/ajchem.2023.28287

$MgAl_2O_4:Ho^{3+}$ Nanophosphors: Electrochemical Sensor, Photoluminescence and Photocatalytic Applications

S.N. Manjula[1,2], M. Chandrasekhar[2,*], M.R. Anil Kumar[3], N. Raghavendra[2], C.R. Ravikumar[2,*], H.C. Ananda Murthy[4,5] and H. Nagabhushana[6]

[1]Department of Physics, SJR College for Women, Rajajinagar, Bengaluru-560010, India
[2]Research Center, Department of Science, East West Institute of Technology, (Affiliated to Visvesvaraya Technological University), Bangalore-560091, India
[3]Department of Chemical and Materials Engineering, Gina Cody School of Engineering and Computer Science, Concordia University, Montreal, Canada, H3G 2W1
[4]Department of Applied Chemistry, School of Applied Natural Science, Adama Science and Technology University, PO Box 1888, Adama, Ethiopia
[5]Department of Prosthodontics, Saveetha Dental College & Hospital, Saveetha Institute of Medical and Technical Science (SIMATS), Saveetha University, Chennai-600077, India
[6]Prof. C.N.R. Rao Center for Advanced Materials, Tumkur University, Tumkur-572103, India

*Corresponding authors: E-mail: mcshekar7@gmail.com; ravicr128@gmail.com

Received: 15 July 2023; *Accepted*: 26 August 2023; *Published online*: 31 October 2023; AJC-21420

Ho^{3+}-doped $MgAl_2O_4$ nanophosphors (1-11 mol%) was synthesised *via* solution combustion method using oxalyl dihydrazide (ODH) as fuel. The findings revealed a range of band gap energies (E_g) between 4.86 and 5.42 eV. It was confirmed that these values correspond extremely well with the experimental data using the DFT approach. The Ho^{3+} ions in the host undergo *f-f* transitions that are triggered at 406 nm and as a result, exhibit discrete photoluminescence emission peaks between 406 and 605 nm. Enhanced $MgAl_2O_4$ have CIE coordinates from orange-red to yellow region and 97% colour purity. Photocatalytic properties of nanophosphors under UV light led to the discovery that a rapid orange-red dye is activated at 493 nm. Removal of fast orange red (F-OR) dye using the new photocatalysts and $MgAl_2O_4:Ho^{3+}$ nanophosphors has been demonstrated. The investigation showed that 89.02% of the dye lost its colour after being exposed to radiation for 120 min. The modified $MgAl_2O_4:Ho^{3+}$ carbon paste electrode used in the cyclic voltametric (CV) technique for lead pollution detection. Based on their electrochemical performance, it is concluded that $MgAl_2O_4:Ho^{3+}$ nanophosphors are a viable material for lead detecting electrodes.

Keywords: Nanophosphors, $MgAl_2O_4:Ho^{3+}$, Solution combustion, Fast orange red dye, Photocatalysis, Electrochemical sensor.

INTRODUCTION

In last several periods, hosts doped with lanthanide ions have allowed scientists to discover new types of brilliant materials. Solid-state lasers, lamps, solar cells, white light-emitting diodes (LEDs) and other technologies all make use of these materials [1-5]. In recent years, there has been significant studies conducted on aluminate materials as phosphors for application in advanced displays and lighting systems. Due to their high dielectric constant, high optical transparency, high thermal stability and resistance to chemical attack, magnesium-aluminum oxide ($MgAl_2O_4$) spinel crystals have been studied as one of these materials [6,7]. Optical, thermal, chemical, mechanical and dielectric characteristics of $MgAl_2O_4$ spinel, a binary compound composed of MgO and Al_2O_3, were found to be exceptional [8]. Powder phosphor containing Dy^{3+}, Eu^{3+}, and Tb^{3+} was synthesized by Omkaram *et al.* [9,10] by a high temperature solid-state chemical method. These creators have investigated the powder phosphors' structure, morphology, and optical properties. Since then, several researchers have worked to perfect the synthesis of $MgAl_2O_4$ nanophosphors using several methods that vary in their starting materials, calcination temper-

atures and other parameters [11]. $MgAl_2O_4:Mn^{2+}$, Cr^{3+} phosphor materials were synthesized *via* solid-state and calcined at 1400 ºC (12 h) [12]. The $MgAl_2O_4:Cr^{3+}$ phosphors were synthesized by Pechini method after being heated to temperatures between 700 and 1200 ºC [13]. The $MgAl_2O_4:Cr^{3+}$ nanophosphor was prepared at 450 ºC using low temperature and high pressure method [14].

Additionally, $MgAl_2O_4:Mn^{2+}$, $MgAl_2O_4$:Bi and $MgAl_2O_4$: Ni^{2+} may be produced synthetically [15-17]. In addition, $^5D_o \rightarrow {}^7F_J$ ($J = 0, 1, 2, 3$ and 4) transitions [18] show that $MgAl_2O_4$ doped with rare-earth metals are highly promising material. $MgAl_2O_4:Tb^{3+}$ are produced using solid-state reaction technology at a temperature of 1220 ºC [19].

$MgAl_2O_4:Eu^{3+}$ and Dy^{3+} phosphors were developed by sol-gel method and they were calcined for 5 h between 600 and 900 ºC [20]. Using a variety of techniques, doped $MgAl_2O_4$ phosphors containing Dy^{3+}, Tb^{3+} and Eu^{3+} have also been synthesized [21-24]. Recent study has demonstrated that red emission of Eu-doped phosphors caused by $^5D_o \rightarrow {}^7F_J$ transitions. Recently, the solution combustion synthesis (SCS) technique was used to synthesize a $MgAl_2O_4$ nanophosphor in range of 1 :1mol% doped with Sm^{3+} [25]. The photocatalytic, photoluminescent, and electrochemical sensor capabilities of $MgAl_2O_4$: Ho^{3+} nanopowders are thoroughly covered in this study.

EXPERIMENTAL

Synthesis of $MgAl_2O_4$: Synthesis of $MgAl_2O_4$ using oxydihydrazide (ODH) as fuel required the use of a redox mixture consisting of magnesium nitrate ($Mg(NO_3)_2{\cdot}6H_2O$) and aluminium nitrate ($Al(NO_3)_3{\cdot}9H_2O$) in stoichiometric proportions. The reactants and double distilled water are mixed in a petri dish and agitated at 400 rpm by magnetic stirrer for 15 min. After preheating muffle furnace to 270 ºC, the mixture was poured inside with the door left open so that oxygen could be introduced to the combustion process. After being ignited, the solution burnt completely for a short while and agate mortar was used to grind the product into powder [26]. This method has been used to develop new nanocrystalline powders because it can make a homogeneous product without the use of high-temperature furnaces.

Preparation of $Mg_{1-x}Al_2O_4:Ho^{3+}$: Synthesis of Ho^{3+} (1-11 mol%) doped with $MgAl_2O_4$ nanophosphors using $Ho(NO_3)_3{\cdot}6H_2O$, $Mg(NO_3)_2{\cdot}6H_2O$ and $Al(NO_3)_3{\cdot}9H_2O$. The ODH was used as fuel in the synthesis process. After that, all the precursors on a petri dish were placed containing little deionized water as possible and heated it to 270 ºC. Combustion byproducts were collected and milled into a powder. Assuming full combustion of redox mixture, the synthesis of $MgAl_2O_4$ were presented as follows:

$$Mg(NO_3)_3{\cdot}6H_2O + 2Al(NO_3)_3{\cdot}9H_2O + xHo(NO_3)_3{\cdot}6H_2O + 4C_2H_6N_4O_2 \longrightarrow Mg_{1-x}Al_2O_4{:}xHo^{3+} + 13N_2 + 33H_2O + 8CO_2 + O_2 \quad (1)$$

RESULTS AND DISCUSSION

PXRD studies: Both pure and Ho^{3+}-doped $MgAl_2O_4$ nanophosphors were subjected to PXRD analysis (Fig. 1). Without any other impurity peaks, each pattern was an ideal fit for the pure cubic phase with the space group *Fd3m* [27] and the JCPDS card no. 21-1152. Since, the structure of $MgAl_2O_4$ was not changed by the limited amount of Ho^{3+} doping and since pure $MgAl_2O_4$ can be produced even at the comparatively low furnace temperature of 270 ± 10 ºC [28]. In the host lattice, Ho^{3+} ions were effectively doped at Mg^{2+} sites rather than interstitial areas. According to calculations, the cubic $MgAl_2O_4$ lattice properties and unit cell volume are, respectively, 8.067 cm^3 and 525.095, respectively. The average crystallite size (eqn. 2) was determined to be between 25 and 42 nm based on the FWHM of the diffraction peaks [20,28].

$$D = \frac{0.9\lambda}{\beta\cos\theta} \quad (2)$$

where D = average crystallite size, λ = X-ray radiation wavelength; β = full-width half-maximum.

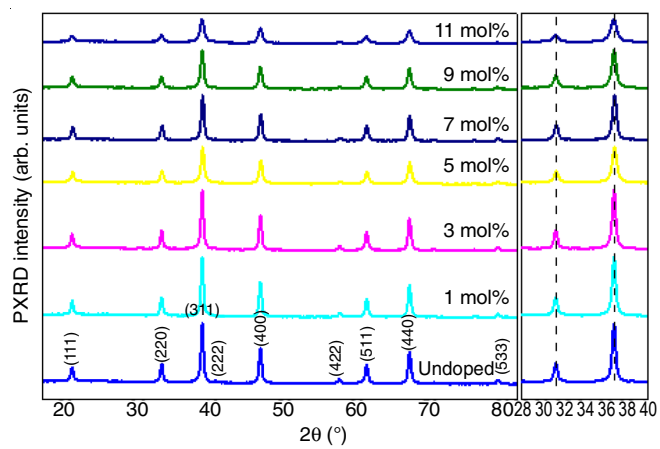

Fig. 1. PXRD of $MgAl_2O_4:Ho^{3+}$ (1-11 mol %) nanophosphors

Addition of Ho^{3+} ions increases peak intensity, suggesting that the sample becomes more crystalline and that the unit cell expands (d value increases). As seen in Fig. 1, this results in PXRD peaks gradually shifting to the side with lower angles. This demonstrates crystal structure of the host matrix isn't random, but rather significantly influenced *via* lattice parameters [20].

DRS studies: Fig. 2a shows the DRS of $MgAl_2O_4:Ho^{3+}$ nanomaterials with concentrations ranging from 1-11 mol%. Spin-allowed 3d-3d transitions of Ho^{3+} ions, $^5I_8 \rightarrow {}^5G_5$ and $^5I^8 \rightarrow {}^5F_5$, generates broad absorption bands at 450 and 646 nm, respectively. Energy gap (E_g) in the optical spectrum was determined using the Kubelka-Munk formula (eqn. 3) [29,30].

$$F(R) = \frac{(1-R)2}{2R} \quad (3)$$

where F(R) = Kubelka-Munk function, R = sample's absolute reflectance.

Increase in Ho^{3+} concentrations may be due to Burstein-Moss effect, action of Ho^{3+} ions on the renormalization of the band gap or the regular drop in E_g values from 3.72 to 3.89 eV (Fig. 2b). This result is consistent with other results [31,32] and due to effect of [Ho-O] clusters on electronic structure of

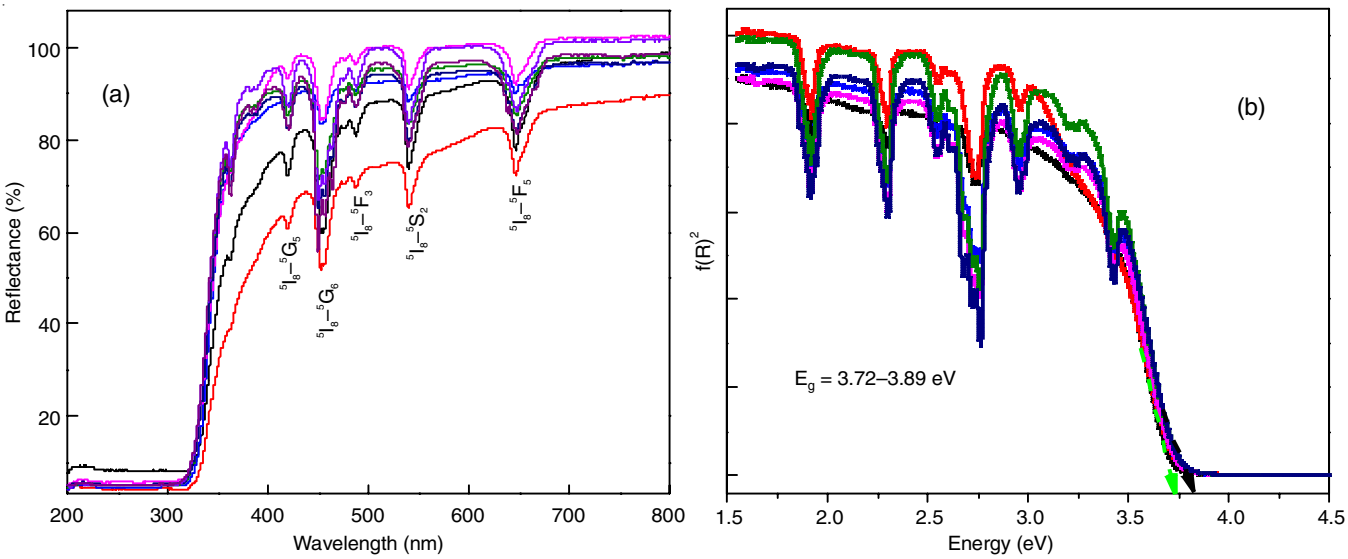

Fig. 2. DRS (a) and energy-gap (b) analysis of $MgAl_2O_4:Ho^{3+}$ (1-11 mol%) nanophosphors

host materials or production of non-bridging oxygens (NBO) brought on by doping.

FTIR studies: Fig. 3 exhibits the FTIR spectra of $MgAl_2O_4:Ho^{3+}$ nanophosphors with concentrations ranging from 1 to 11 mol%. A peak at 532 cm^{-1} assigned for AlO_6 octahedral (ν_4) coordination state, whereas peak at 696 cm^{-1} ascribed to Mg-O band, where 4-asymmetric deformation vibrations [33]. The stretching of Al-O (ν_3) was asymmetrical, which caused the peak at 1018 cm^{-1}. The 1748 and 3453 cm^{-1} peaks were previously ascribed to H-O-H bending vibration and O-H stretching vibration may cause by adsorbate water molecules. Stretching modes C=O and -C=C- was found to be source of the bands between 1500 and 1400 cm^{-1}. Another peak at 2368 cm^{-1} formed when ambient CO_2 was absorbed by the metallic cations, while peaks at 2920 and 2845 cm^{-1} are due to the C-H stretching modes.

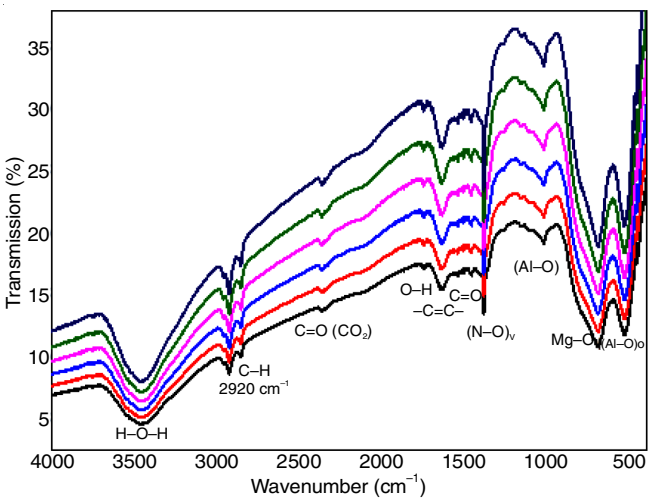

Fig. 3. FT-IR spectra (1-11 mol%) of $MgAl_2O_4:Ho^{3+}$ nanophosphors

Photoluminescence (PL) studies: Excitation spectra for nanophosphor $MgAl_2O_4:Ho^{3+}$ (3 mol%) are shown in Fig. 4. Ho^{3+} ions in cubic symmetry exhibit the spin-allowed transitions $^5I_8 \rightarrow {}^5G_5$, $^5I_8 \rightarrow {}^5F_6$ and $^5I_8 \rightarrow F_3$ which are corresponding to the peaks seen at 416, 450 and 480 nm. It is a possibility that energy radiation in the NUV range can drive the phosphor, making it suitable for use in solid-state displays.

After 450 nm excitation, the PL spectra show a yellow emission band (Fig. 4), which is due to *f-f* transitions of Ho^{3+} from its excited state, $^5I_8 \rightarrow {}_5G_5$. The intense R band at 654 nm results from hypersensitive $^5I_8 \rightarrow {}^5F_3$ forced electric dipole transition of a single Ho^{3+} ion an inversion octahedron (Mg (I) site). The $Mg_2SiO_4:Ho^{3+}$ was also found to have the same emission characteristic [34]. Al^{3+} ions in position 16 are coordinated by a trigonally deformed octahedron (D_{3d} symmetry), whereas Mg^{2+} ions in position 8a are coordinated by a tetrahedron. Octahedral Ho^{3+} are doped into trigonally distorted CrO_6 octahedron, which surrounded by 6 Al^{3+} and 6 Mg^{2+} ions. Weaker lines nearby R band, known as N-lines, may be caused by a pair of Ho^{3+} ions that are strongly connected to one another. The R band is linked to the conventional spinel 16d location. However, Mg^{2+} and Al^{3+} switching positions in the first two coordination spheres may have messed up the Ho^{3+} ions, which may be responsible for the N lines [35].

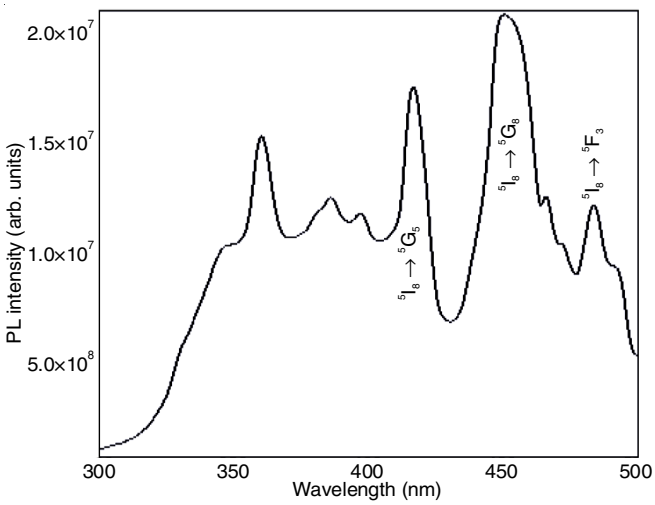

Fig. 4. Excitation spectra of $MgAl_2O_4:Sm^{3+}$ 5 mol% nanophosphors NPs

Emission intensity is clearly affected by Ho^{3+} concentration (9 mol%), and then increases to reach maximum value at 3 mol% concentrations. The luminescence intensity then gradually decreases as a result of concentration quenching due to a variety of defects. By doping $MgAl_2O_4$ with Ho^{3+} ions in place of Mg^{2+}, numerous oxygen vacancies (Vo), single ionized Mg interstitial ($Mg_i^{\blacksquare}$), and ionized Mg (V'_{Mg}) defects were formed.

A negatively charged cation vacancy defect (V'_{Mg}) would balance out positive defects, which correspond to red emission, in order to maintain electroneutrality for the replacement of Ho^{3+} on Mg^{2+} in $MgAl_2O_4$:Ho^{3+}. Additionally, one Mg vacancy (V_{Mg}) would be formed by the negatively charged, singly ionized Mg interstitial ($Mg_i^{\blacksquare}$).

In order to maintain electroneutrality for replacement of Ho^{3+} on Mg^{2+} in $MgAl_2O_4$:Ho^{3+}, a cation vacancy defect (V'_{Mg}) with a negative charge would balance out the created positive defects which correspond to red emission. Additionally, one Mg vacancy (V'_{Mg}) would be formed by the negatively charged, single ionized Mg interstitial ($Mg_i^{\blacksquare}$). Eqns. 4 and 5 may be used to represent the full process.

$$3Mg^{2+} \longrightarrow 2Ho^{3+} + 2Ho^{\blacksquare}_{Mg} + 2V'_{Mg} \quad (4)$$

$$V'_{Mg} + Mg_i^{\blacksquare} \longrightarrow V_{Mg} \quad (5)$$

Doping $MgAl_2O_4$ with Ho^{3+} ions generate defects because it introduces a new defect level by exchanging Mg^{2+} ions for Ho^{3+} ions. When there were temperature fluctuations, the defect's electrons went through a transition to the ground state and emitted red light.

Number of defects is more than the number of filled defects at low concentrations, but when Ho^{3+} concentration increases, the quantity of Mg^{2+} ions falls and the number of defects decreases. Consequently, red emission intensity decreases as doping concentrations increase [36]. Energy transfer contact types were determined using the Van-Uitert hypothesis [26]. A linear fitting yielded a value of 3 mol%, suggesting that an exchange interaction was responsible for concentration quenching of $MgAl_2O_4$:Ho^{3+} phosphor (Fig. 5).

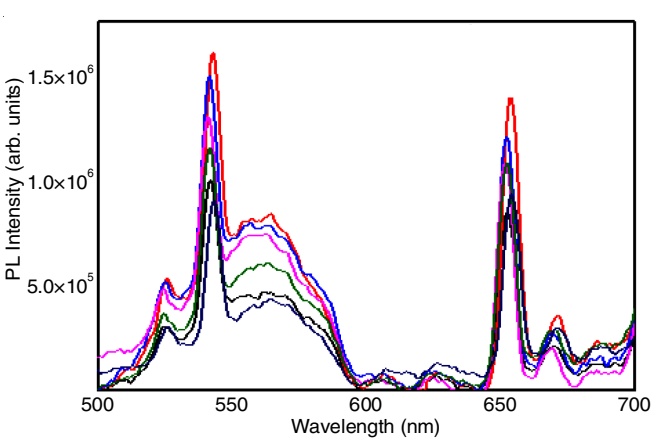

Fig. 5. Emission spectra of $MgAl_2O_4$:Ho^{3+} (1-11 mol %) nanophosphors

Colour perception of light-emitting $MgAl_2O_4$:Ho^{3+} nanostructures were determined using the CIE's 1931 chromaticity coordinate diagram [37]. By analyzing the 406 nm-stimulated emission spectra, we were able to identify that $MgAl_2O_4$:Ho^{3+} nanostructures fall within the CIE chromaticity coordinates for orange-red to yellow (Fig. 6). This hints to a prospective user for all-purpose light sources [38,39] (orange-red to yellow light). This discovery suggests the phosphor has great potential usage for white LEDs and other solid-state display usage to provide artificial white light.

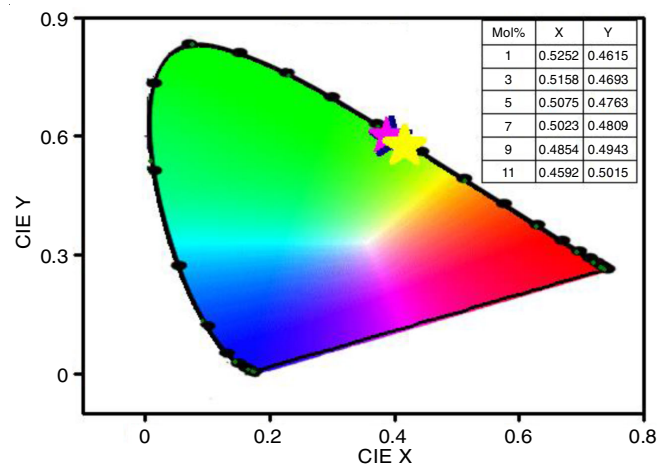

Fig. 6. CIE graph of $MgAl_2O_4$:Ho^{3+} (1-11 mol %) nanophosphors (406 nm)

Photocatalytic analysis: Fast orange red (FOR) dye degradation was examined after ODH utilized as fuel in UV light irradiation method to produce $MgAl_2O_4$:Ho^{3+} nanophosphors. The reaction mixture contained 60 mg of photocatalyst and 20 ppm of dye. At predetermined times throughout the reaction, 5 mL dye solution was removed, centrifuged to separate photocatalyst [40] and absorbance of the resulting dye samples was measured at 493 nm. Using $MgAl_2O_4$:Ho^{3+}, the photocatalytic decolorization of dye at 120 min reveals greater percentage (89%) among all mol% of $MgAl_2O_4$:Ho^{3+} 9 mol%. As photocatalyst, $MgAl_2O_4$ doped with 9 mol% Ho^{3+} efficiently degrades FOR dye. The breakdown of $MgAl_2O_4$:Ho^{3+} dye by ultraviolet light (1-11 mol%) is observed in the UV absorption spectrum (Fig. 7). The percentage of deterioration was calculated using eqn. 6:

$$D\ (\%) = \frac{C_o - C}{C_o} \times 100 \quad (6)$$

where % D = photo decolorization efficiency, C_o and C = the initial and final dye solution concentration, respectively.

Fig. 8a displays a proportion of decolorization of $MgAl_2O_4$:Ho^{3+} (1-11 mol%) nanophosphors during UV light irradiation for FOR dye. When compared to other mol% of nanophosphors, 9 mol% Ho^{3+}-doped $MgAl_2O_4$ nanophosphor sample clearly demonstrates the best photodecolorization efficiency. After 120 min of irradiation, the percentage decolorization rate for the FOR dye reaches as high as 89%, and this rate rises in tandem with the Ho^{3+} concentration. It has been observed that Langmuir-Hinshelwood model (eqn. 7) can be used to quantitatively learn response kinetics of FOR dye decolorization:

$$\ln\left(\frac{C}{C_o}\right) = kt + a \quad (7)$$

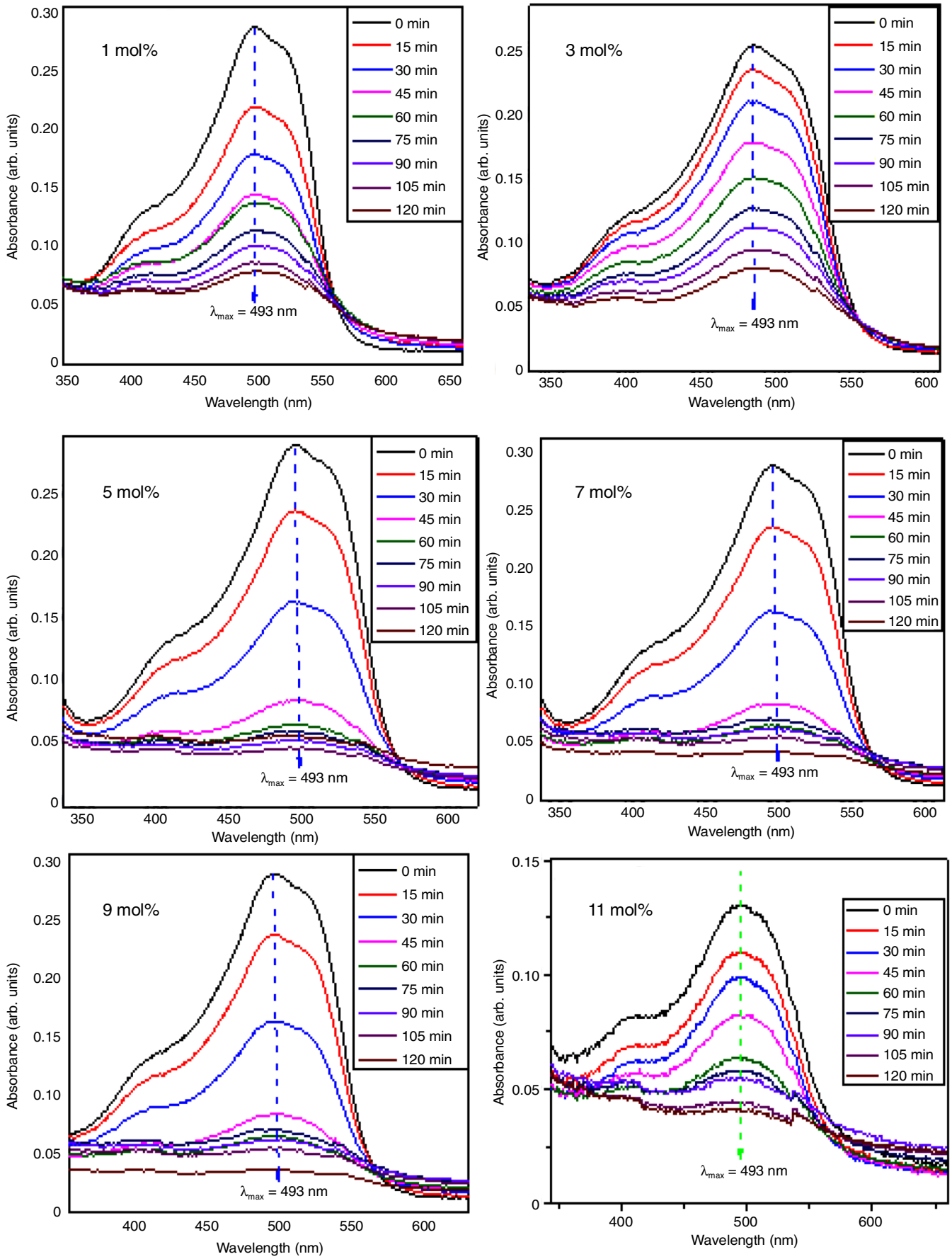

Fig. 7. UV-Vis absorption spectra of $MgAl_2O_4:Ho^{3+}$ (1-11 mol %) for FOR dye under UV light

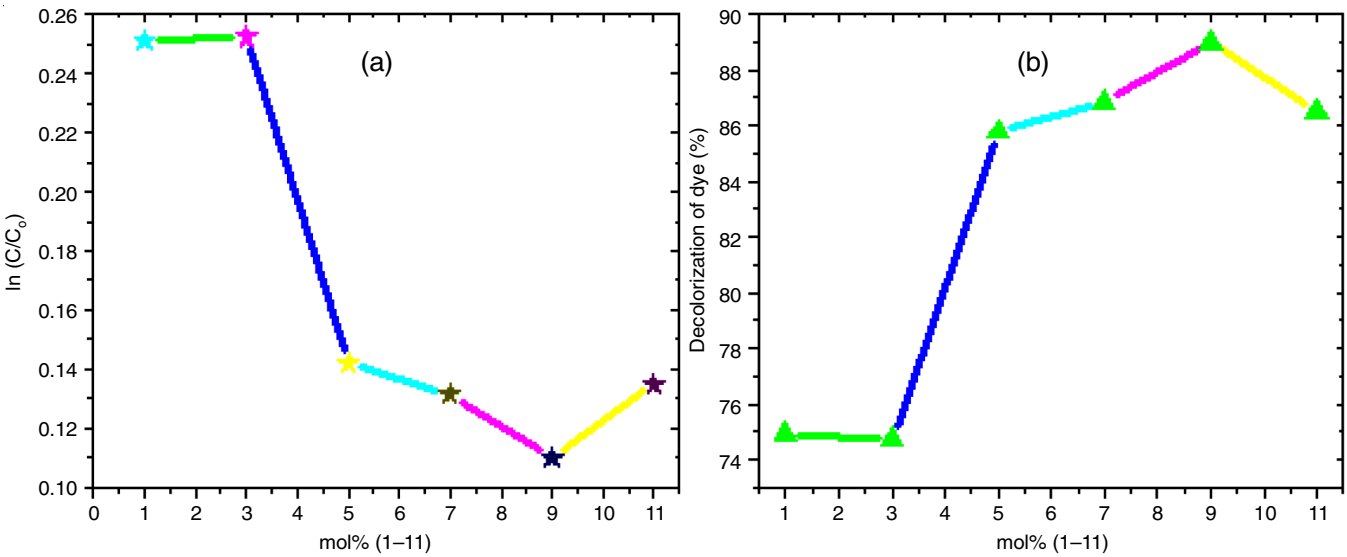

Fig. 8. (a) log C/C$_o$ and (b) % Degradation of $MgAl_2O_4$:Ho^{3+} (1-11 mol %) FOR dye under UV light

where k = reaction rate constant, C_o = initial concentration of dye, and C = concentration of dye at time t.

Absorption studies have shown that an increase in charge carrier separation and an increase in the generation of hydroxyl radicals are the primary causes of dye decolorization.

A plot of log (C/C$_o$) against mol% (Fig. 8b) reveals the degradation rate increased with increasing mol% for 120-min. The log C/C$_o$ values was computed using eqn. 7, which was utilized in the process.

$$\log \frac{C}{C_o} = -Kt \quad (7)$$

where, C_o and C are the initial and final concentration of dye at time t = 0 min; and k is the first order rate constant.

Results of the kinetics study and % decolorization are shown in Table-1. This suggests that $MgAl_2O_4$ doped with 9 mol% of Ho^{3+} is the most effective photocatalyst degradation of FOR dye followed by 7, 11, 5, 3 and 1 mol%.

TABLE-1
RATE CONSTANTS AND KINETIC STUDIES OF FAST ORANGE RED (FOR) DYE DECOLORIZATION UNDER UV LIGHT

20 ppm FOR dye + 60 mg $MgAl_2O_4$:Ho^{3+} (1-11 mol %) + UV					
Mol %	c	c/c$_o$	log c/c$_o$	-log c/c$_o$	D (%)
0	20	1	0	0	0
1	2.511	0.2511	-0.60015	0.6001	74.89
3	2.523	0.2523	-0.59808	0.5980	74.77
5	1.422	0.1422	-0.8471	0.8471	85.78
7	1.314	0.1314	-0.8814	0.8814	86.86
9	1.104	0.1121	-0.9586	0.9586	89.02
11	1.352	0.1351	-0.8690	0.8690	86.48
			Slope	0.00262	
			Rate	0.00604	

Cyclic voltammetry studies: Fig. 9 displays the CV results of $MgAl_2O_4$ with different extramol concentrations of Ho^{3+} along with electrode's charge-discharge cycle, reaction reversibility, oxygen evolution property, charge efficiency and other factors were presented. The difference between oxidation and reduction potential ($E_O - E_R$) may be used to gauge how reversible an electrode reaction is; a lower difference indicates a greater reversible electrode reaction [41].

Table-2 displays the $MgAl_2O_4$ electrode with a 9 mol% concentration. The electrochemical reaction of Ho^{3+} exhibits a limited degree of reversibility and a prolonged oxidation-reduction peak separation. But it is evident that adding Ho^{3+} as a dopant changes the CV curve of $MgAl_2O_4$ electrode.

TABLE-2
OXIDATION POTENTIAL, REDUCTION POTENTIAL AND THE DIFFERENCE b/w OXIDATION & REDUCTION POTENTIAL OF DIFFERENT ELECTRODES

Name of the electrode	EO (V)	ER (V)	EO-ER (V)
$MgAl_2O_4$ (1 mol%)	-0.1117	-0.4049	0.2932
$MgAl_2O_4$ (3 mol%)	-0.1108	-0.3706	0.2598
$MgAl_2O_4$ (5 mol%)	-0.2209	-0.4627	0.2418
$MgAl_2O_4$ (7 mol%)	-0.2442	-0.4622	0.2380
$MgAl_2O_4$ (9 mol%)	0.1904	-0.3667	0.1763
$MgAl_2O_4$ (11 mol%)	-0.2198	-0.4611	0.2413

Steady-state electrochemical impedance spectra (EIS) of $MgAl_2O_4$:Ho^{3+} electrodes (1- 11 mol%) after activation during CV measurement (Fig. 9). The impedance spectra of these six electrodes exhibit low-frequency slope associated with the Warburg impedance [42] and a high-frequency depressed semi-circle associated with charge transfer resistance (R_{ct}). As seen in Fig. 10, $MgAl_2O_4$ linked with a (9 mol%) Ho^{3+} electrode displays much bigger capacitive arches than other electrodes. Ho^{3+} (9 mol%) may entirely reduce the R_{ct} value and electrochemical process in $MgAl_2O_4$ electrodes, in contrast to Ho^{3+}-doped $MgAl_2O_4$ electrode concentrations of 1-11 mol%.

Lead was discovered using a modified carbon paste electrode and CV of $MgAl_2O_4$:Ho^{3+} (9 mol%, 10 mV/s scan rate) nano-phosphors (Fig. 11a-e). The sensing performance of $MgAl_2O_4$:Ho^{3+} was evaluated using lead concentrations ranging from 1 to 5 mM. In absence of lead, oxidation and reduction maxima occurred at -0.225 V and -0.412 V, respectively. In presence of lead, oxidation peak changes from -0.225 V to -0.524 V while

Fig. 9. CV of $MgAl_2O_4:Ho^{3+}$ electrodes (1-11%) at various scan rates in 0.1 N HCl electrolyte *vs.* Ag/AgCl electrode

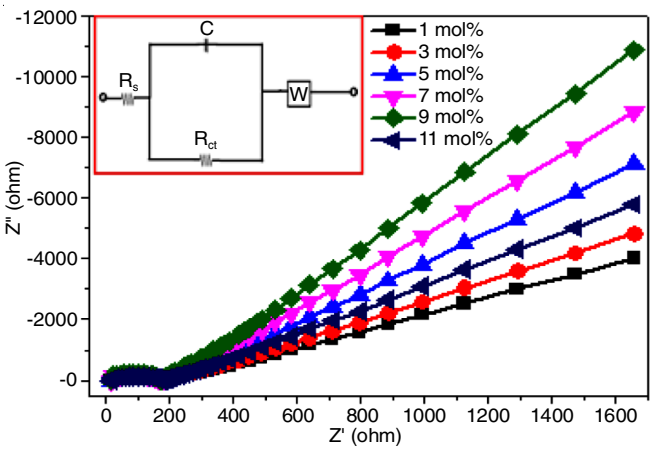

Fig. 10. Electrochemical impedance spectra of $MgAl_2O_4:Ho^{3+}$ electrodes (1-11 mol%) and equivalent circuit

reduction peak shifts from -0.412V to -0.649V and -0.973 V. It is confirmed that the synthetic $MgAl_2O_4:Ho^{3+}$ oxidized the lead at -0.412 V and lowered it at -0.649 and -0.973 V. Using a calibration curve, Fig. 12 shows peak current as function of lead concentration. Low detection limit of $MgAl_2O_4:Ho^{3+}$ electrode was established to be 1×10^{-3} mol/L. Linear nature of calibration curve indicates that the activity is diffusion controlled in specified concentration range [42]. This demonstrates the improved electrochemical sensitivity of $MgAl_2O_4:Ho^{3+}$-modified electrodes.

Conclusion

$MgAl_2O_4:Ho^{3+}$ nanophosphors were synthesized by burning oxalyl dihydrazide (ODH) at low temperatures as a convincing fuel. These nanophosphors contain 20 nm sized crystallites on average with band gaps that range from 3.72 to 3.89 eV.

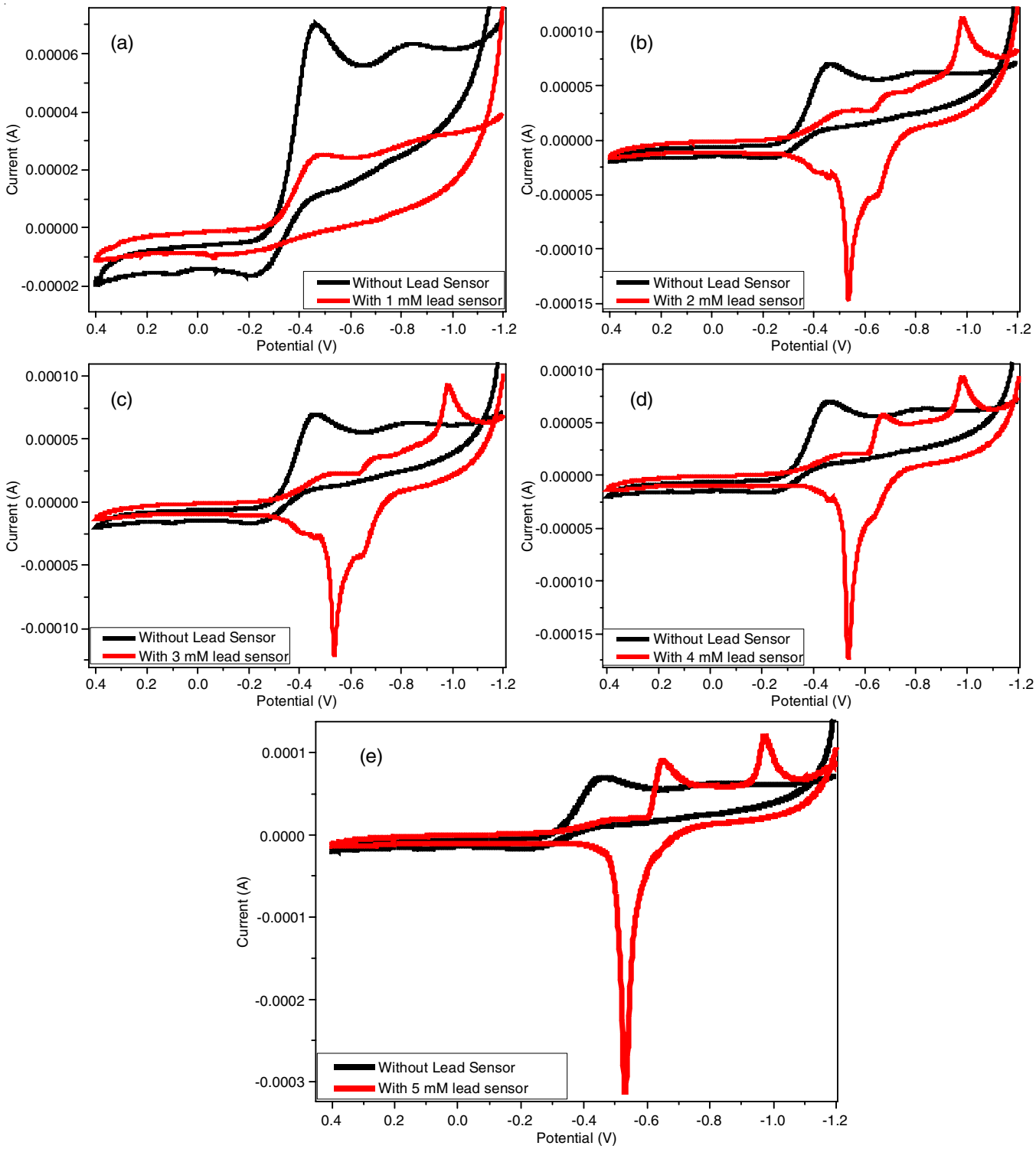

Fig. 11. CV of $MgAl_2O_4:Ho^{3+}$ (9 mol%, scan rate - 10 mV/s) for sensing of lead concentration range (1-5 mM)

Due to specific transitions from $^4F_{7/2} \rightarrow {}^6P_{3/2}$, which were brought on by *f-f* transitions of Ho^{3+} ions in the host and the distinctive photoluminescence emission peaks of Ho^{3+} ions were found in the range of 406 and 605 nm. The ideal $MgAl_2O_4$ phosphors were found to have a 97% colour purity and CIE coordinates, which are in the orange-red-yellow zone. After 120 min of radiation, the experiment revealed 89% dye decolorization. A modified carbon paste electrode and the CV technique were used to detect lead in 0.1 N HCl solution (MCPE). According to electrochemical performance, $MgAl_2O_4:Ho^{3+}$ nanophosphors are effective sensing electrode materials for elements like lead.

CONFLICT OF INTEREST

The authors declare that there is no conflict of interests regarding the publication of this article.

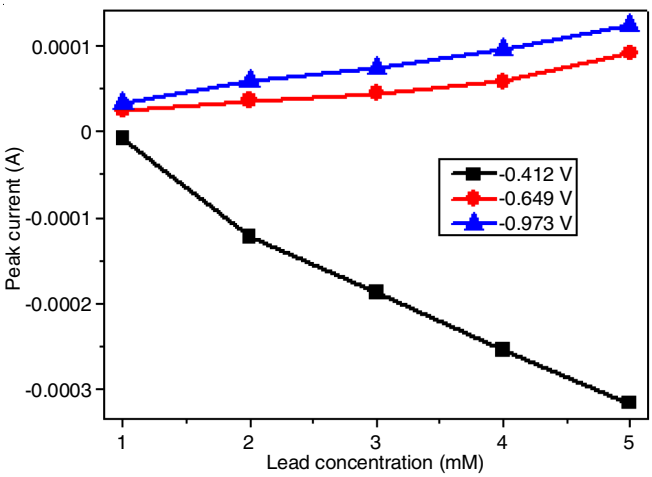

Fig. 12. Calibration plot of peak current against lead concentration (1-5 mM)

REFERENCES

1. J. Wrzyszcz, W. Miœta, D. Hreniak, W. Strek, M. Zawadzki and H. Grabowska, *J. Alloys Compd.*, **341**, 358 (2002); https://doi.org/10.1016/S0925-8388(02)00037-3
2. L.H. Brixner and P.A. Flournoy, *J. Electrochem. Soc.*, **112**, 303 (1965); https://doi.org/10.1149/1.2423528
3. L.D. Merkle, A. Pinto, H.R. Verdún and B. McIntosh, *Appl. Phys. Lett.*, **61**, 2386 (1992); https://doi.org/10.1063/1.108172
4. H.Y. Lin, W.F. Chang and S.Y. Chu, *J. Lumin.*, **133**, 194 (2013); https://doi.org/10.1016/j.jlumin.2011.12.034
5. J. Zhao, C. Guo, J. Yu and R. Yu, *Opt. Laser Technol.*, **45**, 62 (2013); https://doi.org/10.1016/j.optlastec.2012.07.032
6. V. Singh, M.D.M. Haque and D.-K. Kim, *Bull. Korean Chem. Soc.*, **28**, 2477 (2007); https://doi.org/10.5012/bkcs.2007.28.12.2477
7. O. Padmaraj, M. Venkateswarlu and N. Satyanarayana, *Ceram. Int.*, **41**, 3178 (2015); https://doi.org/10.1016/j.ceramint.2014.10.169
8. S.M. Hosseini, *Phys. Stat. Sol. (b)*, **245**, 2800 (2008); https://doi.org/10.1002/pssb.200844142
9. I. Omkaram and S. Buddhudu, *Opt. Mater.*, **32**, 8 (2009); https://doi.org/10.1016/j.optmat.2009.05.010
10. I. Omkaram, B. Vengala Rao and S. Buddhudu, *J. Alloys Compd.*, **474**, 565 (2009); https://doi.org/10.1016/j.jallcom.2008.06.140
11. I. Ganesh, *Int. Mater. Rev.*, **58**, 63 (2013); https://doi.org/10.1179/1743280412Y.0000000001
12. Q. Sai, C. Xia, H. Rao, X. Xu, G. Zhou and P. Xu, *J. Lumin.*, **131**, 2359 (2011); https://doi.org/10.1016/j.jlumin.2011.05.046
13. P. Gluchowski, R. Pazik, D. Hreniak and W. Strêk, *Chem. Phys.*, **358**, 52 (2009); https://doi.org/10.1016/j.chemphys.2008.12.018
14. P. Gluchowski and W. Strek, *Mater. Chem. Phys.*, **140**, 222 (2013); https://doi.org/10.1016/j.matchemphys.2013.03.025
15. W.A.I. Tabaza, H.C. Swart and R.E. Kroon, *J. Lumin.*, **148**, 192 (2014); https://doi.org/10.1016/j.jlumin.2013.12.018
16. V. Singh, R.P.S. Chakradhar, J.L. Rao and D.K. Kim, *J. Solid State Chem.*, **180**, 2067 (2007); https://doi.org/10.1016/j.jssc.2007.04.030
17. A. Jouini, A. Yoshikawa, Y. Guyot, A. Brenier, T. Fukuda and G. Boulon, *Opt. Mater.*, **30**, 47 (2007); https://doi.org/10.1016/j.optmat.2006.11.027
18. R. Sakai, T. Katsumata, S. Komuro and T. Morikawa, *J. Lumin.*, **85**, 149 (1999); https://doi.org/10.1016/S0022-2313(99)00061-7
19. I. Omkaram, G. Seeta Rama Raju and S. Buddhudu, *J. Phys. Chem. Solids*, **69**, 2066 (2008); https://doi.org/10.1016/j.jpcs.2008.03.005
20. A.S. Maia, R. Stefani, C.A. Kodaira, C.F.C. Felinto, E.E.S. Teotonio and H.F. Brito, *Opt. Mater.*, **31**, 440 (2008); https://doi.org/10.1016/j.optmat.2008.06.017
21. Y. Lu, J. Wang, L. He, C. Hao, F. Wang and J. Zhang, *Mater. Res. Express*, **9**, 065009 (2022); https://doi.org/10.1088/2053-1591/ac7b72
22. R.J. Wiglusz and T. Grzyb, *Opt. Mater.*, **33**, 1506 (2011); https://doi.org/10.1016/j.optmat.2011.04.020
23. Y. Lu, J. Wang, Z.X. Shi, L.J. Dai, H.M. Zhang, Z.T. Sun and Y.F. Liu, *Chinese J. Inorg. Chem.*, **36**, 688 (2020).
24. Q.U. Ain, B. Ismail, A.M. Khan, R.A. Khan, F. Shah, Hafiz-Ur Rehman and F. Shahid, *Semicond. Sci. Technol.*, **36**, 125010 (2021); https://doi.org/10.1088/1361-6641/ac2750
25. S. Ashwini, S.C. Prashantha, R. Naik, Y.V. Naik, H. Nagabhushana and K.N. Narasimhamurthy, *J. Sci. Adv. Mater. Devices*, **4**, 531 (2019); https://doi.org/10.1016/j.jsamd.2019.09.001
26. C. Pratapkumar, S.C. Prashantha, H. Nagabhushana, M.R. Anilkumar, C.R. Ravikumar, H.P. Nagaswarupa and D.M. Jnaneshwara, *J. Alloys Compd.*, **728**, 1124 (2017); https://doi.org/10.1016/j.jallcom.2017.09.058
27. Z. Wang, S. jiao, Y. Xu, Q. Zhang, Y. Chen, G. Pang and S. Feng, *J. Lumin.*, **211**, 108 (2019); https://doi.org/10.1016/j.jlumin.2019.03.008
28. Z.G. Lei, D.W. Meng, Z.X. Gao, X.L. Zhang, Q.X. Yang and Y.Q. Wang, *J. Mater. Sci. Mater. Electron.*, **27**, 1840 (2016); https://doi.org/10.1007/s10854-015-3962-7
29. S. Cizauskaite, G. Spakauskaite, A. Beganskiene and A. Kareiva, *Chemija*, **17**, 40 (2006).
30. G.H. Du, Z.L. Liu, X. Xia, Q. Chu and S.M. Zhang, *J. Sol-Gel. Sci.*, **39**, 285 (2006); https://doi.org/10.1007/s10971-006-7780-5
31. M. Chroma, J. Pinkas, I. Pakutinskiene, A. Beganskiene and A. Kareiva, *Ceram. Int.*, **31**, 1123 (2005); https://doi.org/10.1016/j.ceramint.2004.11.012
32. B. Schrader, Infrared and Raman Spectroscopy. Methods and Applications, VCH, Weinheim (1995).
33. H. Shahbazi, H. Shokrollahi and A. Alhaji, *J. Alloys Compd.*, **712**, 732 (2017); https://doi.org/10.1016/j.jallcom.2017.04.042
34. W. Nantharak, W. Wattanathana, W. Klysubun, T. Rimpongpisarn, C. Veranitisagul, N. Koonsaeng and A. Laobuthee, *J. Alloys Compd.*, **701**, 1019 (2017); https://doi.org/10.1016/j.jallcom.2017.01.090
35. S. Sanjabi and A. Obeydavi, *J. Alloys Compd.*, **645**, 535 (2015); https://doi.org/10.1016/j.jallcom.2015.05.107
36. R. Naik, S.C. Prashantha, H. Nagabhushana, S.C. Sharma, H.P. Nagaswarupa and K.M. Girish, *J. Alloys Compd.*, **682**, 815 (2016); https://doi.org/10.1016/j.jallcom.2016.05.037
37. G. Rani, *Powder Technol.*, **312**, 354 (2017); https://doi.org/10.1016/j.powtec.2017.02.040
38. S.K. Sampath, D.G. Kanhere and R. Pandey, *J. Phys. Condens. Matter*, **113**, 635 (1999); https://doi.org/10.1088/0953-8984/11/18/301
39. Q. Bai, P. Li, Z. Wang, S. Xu, T. Li, Z. Yang and Z. Xu, *Spectrochim. Acta A Mol. Biomol. Spectrosc.*, **199**, 179 (2018); https://doi.org/10.1016/j.saa.2018.03.065
40. M.R.A. Kumar, B. Abebe, H.P. Nagaswarupa, H.C.A. Murthy, C.R. Ravikumar and F.K. Sabir, *Sci. Rep.*, **10**, 1249 (2020); https://doi.org/10.1038/s41598-020-58110-7
41. B. Shruthi, B.J. Madhu, V.B. Raju, S. Vynatheya, B.V. Devi, G.V. Jayashree and C.R. Ravikumar, *J. Sci. Adv. Mater. Devices*, **2**, 93 (2017); https://doi.org/10.1016/j.jsamd.2016.12.002
42. B. Avinash, C.R. Ravikumar, M.R.A. Kumar, H.P. Nagaswarupa, M.S. Santosh, A.S. Bhatt and D. Kuznetsov, *J. Phys. Chem. Solids*, **134**, 193 (2019); https://doi.org/10.1016/j.jpcs.2019.06.012